




## Ni(II) and Co(III) complexes of 5-methyl-1,3,4-thiadiazole-2-thiol: syntheses, spectral, structural, thermal analysis, and DFT calculation

R.K. Dani, M.K. Bharty, Om Prakash, Ranjan K. Singh, Billa Prashanth, Sanjay Singh & N.K. Singh


To cite this article: R.K. Dani, M.K. Bharty, Om Prakash, Ranjan K. Singh, Billa Prashanth, Sanjay Singh & N.K. Singh (2015) Ni(II) and Co(III) complexes of 5-methyl-1,3,4-thiadiazole-2-thiol: syntheses, spectral, structural, thermal analysis, and DFT calculation, Journal of Coordination Chemistry, 68:15, 2666-2681, DOI: [10.1080/00958972.2015.1057131](https://doi.org/10.1080/00958972.2015.1057131)

To link to this article: <http://dx.doi.org/10.1080/00958972.2015.1057131>

 View supplementary material 

 Published online: 25 Jun 2015.

 Submit your article to this journal 

 Article views: 94

 View related articles 

 View Crossmark data 

## Ni(II) and Co(III) complexes of 5-methyl-1,3,4-thiadiazole-2-thiol: syntheses, spectral, structural, thermal analysis, and DFT calculation

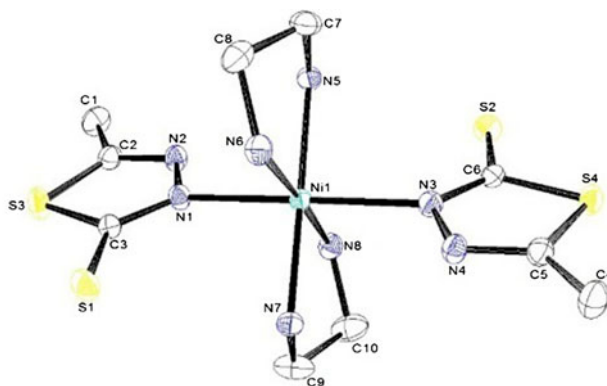
R.K. DANI†, M.K. BHARTY\*‡, OM PRAKASH‡, RANJAN K. SINGH‡,  
BILLA PRASHANTH§, SANJAY SINGH§ and N.K. SINGH\*‡

†Faculty of Science, Department of Chemistry, Banaras Hindu University, Varanasi, India

‡Faculty of Science, Department of Physics, Banaras Hindu University, Varanasi, India

§Department of Chemical Sciences, IISER Mohali, Mohali, India

(Received 9 January 2015; accepted 23 April 2015)



Two new complexes,  $[\text{Ni}(\text{en})_2(\text{mtt})_2]$  (**1**) and  $[\text{Co}(\text{en})_2(\text{mtt})_2](\text{mtt})$  (**2**) (Hmtt = 5-methyl-1,3,4-thiadiazole-2-thiol and en = ethylenediamine), have been synthesized and characterized by various physicochemical techniques. Complexes **1** and **2** crystallize in monoclinic and orthorhombic system with space groups  $P 21/n$  and  $P 21 21 21$ , respectively. The molecular structures of **1** and **2** show that the metal ions are six-coordinate bonded through four equatorial nitrogens of two en and two axial nitrogens of mtt ligands. The crystal structures of the complexes reveal that mtt is present in thione form and bound to the metal ion through the thiadiazole nitrogen. The crystal structures of the complexes are stabilized by various intermolecular hydrogen bonding providing supramolecular architecture. Complex **2** is also stabilized by weak  $\pi \cdots \pi$  interactions occurring between two thiadiazole rings. The bioefficacies of the ligand and complexes have been examined against the growth of bacteria to evaluate their antimicrobial potential. The biological results suggest that **2** is more active than the ligand and **1** against the tested bacteria. The geometries of the ligand and the complexes have been optimized by the DFT method and the results are compared with the X-ray diffraction data. The Co(III) complex exhibits an irreversible Co(III)/Co(II) process while the Ni(II) complex displays quasi-reversible Ni(II)/Ni(III) redox processes with large peak separation as compared to that expected for a one electron process which is thought to be coupled with some chemical reaction.

\*Corresponding authors. Email: [mkbharty@bhu.ac.in](mailto:mkbharty@bhu.ac.in) (M.K. Bharty); [nksingh@bhu.ac.in](mailto:nksingh@bhu.ac.in) (N.K. Singh)

**Keywords:** 1,3,4-Thiadiazole complexes; Ni(II) and Co(III) complexes; Supramolecular architecture; TGA; Antibacterial property; DFT calculation

## 1. Introduction

The syntheses of five-membered heterocyclic ring systems such as 1,3,4-thiadiazole have been undertaken during recent years because of their interesting physiological properties. They exhibit broad spectrum pharmacological properties and their derivatives constitute an important class of organic compounds with diverse agricultural and industrial applications and display antimicrobial, sedative, anticonvulsant, and anti-inflammatory activities [1, 2]. Thiadiazoles have found applications as pharmaceuticals, oxidation inhibitors, cyanine dyes, and metal complexing agents [3]. Transition metal complexes exhibit many features including structures, redox, and physicochemical properties which make them suitable for applications in medicine and biotechnology [4]. Cobalt is an essential trace element present in vitamin B<sub>12</sub> which is essential for human health. Cobalt is associated with important synthetic reactions in the metabolic processes [5]. Nickel is also an essential element present in several enzymes and plays a vital role in physiological processes as a cofactor in the absorption of iron from the intestine [6]. With the biological importance of cobalt and nickel, it is important to study their complexes with bioactive ligands to understand functions of the complexes and to find new bioactive compounds [7, 8]. A number of reports on the antibacterial properties of cobalt complexes have appeared in the literature, with Co(II) complexes being the most studied, presumably due to their aqueous stability, availability, and ease of synthesis. Reports on the antibacterial properties of cobalt(III) complexes frequently emphasize the increased effectiveness of cobalt coordination to a particular ligand when compared with the free ligand itself [9, 10]. One of the most interesting properties of mercapto-substituted thiadiazoles is the existence of thiol–thione tautomerism which influences the reactivity of thiadiazoles in polymerization processes, substitution reactions at the different moieties, and metal complexation [11, 12]. 2,5-Dimercapto-1,3,4-thiadiazole and 2-mercapto-5-methyl-1,3,4-thiadiazole exhibit tautomeric equilibria, and the structures of the compounds by *ab initio* and DFT computations support the thione form as being the most stable [13]. Some work has been reported on complexes of 5-methyl-1,3,4-thiadiazole-2-thiol (=Hmtt), but no work has been reported on its nickel(II) and cobalt(III) complexes containing ethylenediamine (= en) as the coligand [14]. Therefore, we investigate the nickel(II) and cobalt(III) complexes of 5-methyl-1,3,4-thiadiazole-2-thiol containing en as secondary ligand and compare the mode of bonding of the ligand and the structures of the complexes. We have also performed DFT-based calculations to corroborate the experimental results.

## 2. Experimental

### 2.1. Materials and characterization

Commercial reagents were used without purification and all experiments were carried out in an open atmosphere. 5-Methyl-1,3,4-thiadiazole-2-thiol (Sigma-Aldrich), metal acetate, and ethylenediamine (BDH Chemicals) were used as received. All solvents were purchased from Merck Chemicals, India, dried and distilled before use by following standard procedures.

## 2.2. Physical measurements

Carbon, hydrogen, nitrogen, and sulfur contents were estimated on a CHN Model CE-440 Analyzer and on an Elementar Vario EL III Carlo Erba 1108. Magnetic susceptibility measurements were performed at room temperature on a Cahn Faraday balance using Hg[Co(NCS)<sub>4</sub>] as the calibrant and electronic spectra were recorded on a SHIMADZU 1700 UV–vis spectrophotometer in DMSO. IR spectra were recorded from 4000 to 400 cm<sup>-1</sup> as KBr pellets on a Varian Excalibur 3100 FT-IR spectrophotometer. Thermogravimetric analyses were done using a Perkin–Elmer–STA 6000 thermal analyzer in a nitrogen atmosphere at a heating rate of 10 °C min<sup>-1</sup> from 30 to 950 °C.

## 2.3. Antibacterial tests

Five human bacterial pathogens, *Salmonella typhi* (MTCC 3216), *Shigella flexneri* (ATCC 12022), *Staphylococcus aureus* (ATCC 25323), *Aeromonas hydrophila* (ATCC 7966), and *Enterococcus faecalis* (ATCC 25923), were used to test the antibacterial activities of the ligand, M(OAc)<sub>2</sub>·xH<sub>2</sub>O, **1** and **2**. The antibacterial assays were carried out according to the reported method with some slight modifications [15, 16]. The test compounds were dissolved in DMSO to a final concentration of 5 mg/mL. Sterilized Whatman No. 1 filter paper disks (5 mm) were impregnated with different volumes (1, 2, 4, 6, 8, and 10 μL) of compounds to get final concentrations of 5, 10, 20, 30, 40, and 50 μg per disk. Sterilized paper disk loaded with 10 μL of DMSO was taken as a control. The bacterial test pathogens were spread on fresh Mueller Hinton Agar (MHA) plates with the help of cotton swabs to form an even lawn of the test bacteria. The filter paper disks impregnated with the test compounds were placed on the surface of the MHA plates seeded with test bacteria and the plates were incubated in a B.O.D. incubator (Caltan-152, Narang Scientific Works, New Delhi, India) for 24 h at 37 ± 2 °C. The inhibition zone around each disk was measured after 24 h of incubation. Commercial antibacterial drugs streptomycin sulfate and neomycin sulfate (Himedia) were used in the same concentration of 5–50 μg/disc to compare effectiveness of the test compounds.

## 2.4. Synthesis

**2.4.1. Synthesis of [Ni(mtt)<sub>2</sub>(en)<sub>2</sub>] (1).** Ni(OAc)<sub>2</sub>·4H<sub>2</sub>O (0.248 g, 1 mmol) and Hmtt (0.264 g, 2 mmol) were dissolved separately in 20 mL methanol, mixed, and stirred for 1 h. The separated precipitate was filtered, washed with methanol–water mixture (50 : 50), and air dried. The precipitate was suspended in methanol to which ethylenediamine (0.2 mL, 2 mmol) was added and stirred for 2 h. The resulting clear pink solution was filtered and kept for crystallization. Pink crystals of **1** suitable for X-ray analyses were obtained by slow evaporation of the methanol solution over a period of 15 days. Yield: (58%); m.p. 196 °C; Anal. Found: C, 27.17; H, 4.81; N, 25.48; S, 29.14%. Calcd for C<sub>10</sub>H<sub>22</sub>N<sub>8</sub>S<sub>4</sub>Ni (441.25): C, 27.15; H, 4.97; N, 25.39; S, 29.07%. IR (KBr, cm<sup>-1</sup>): ν(NH) 3214, ν(C=N) 1598, ν(N–N) 1070, ν(C=S) 932, ν(Ni–N) 534. UV–vis. [λ<sub>max</sub>, DMSO, nm]: 446, 415 and 324.

**2.4.2. Synthesis of [Co(mtt)<sub>2</sub>(en)<sub>2</sub>](mtt) (2).** Co(OAc)<sub>2</sub> (0.177 g, 1 mmol) and Hmtt (0.396 g, 3 mmol) were dissolved separately in 15–20 mL methanol, mixed, and stirred for 1 h. The separated brown solid was filtered and washed with methanol–water mixture

(50 : 50 v/v) and finally with methanol. A methanol solution (10 mL) of ethylenediamine (0.2 mL, 2 mmol) was added to the methanol suspension of the above compound and stirred for 30 min. A clear dark red solution was obtained, filtered, and kept for crystallization. Reddish brown crystals of **2** suitable for X-ray analyses were obtained by slow evaporation of the above solution over a period of 10 days. Yield: (48%); m.p. 236 °C; Anal. Found: C, 27.24; H, 4.36; N, 24.37; S, 33.54%. Calcd for C<sub>13</sub>H<sub>25</sub>N<sub>10</sub>S<sub>6</sub>Co (572.74): C, 27.39; H, 4.90; N, 24.44; S, 33.52%. IR (KBr, cm<sup>-1</sup>):  $\nu(\text{NH})$  3206,  $\nu(\text{C}=\text{N})$  1605,  $\nu(\text{N}-\text{N})$  1055,  $\nu(\text{C}=\text{S})$  948,  $\nu(\text{Co}-\text{N})$  548. UV-vis. [ $\lambda_{\text{max}}$ , DMSO, nm]: 460, 434 and 332.

## 2.5. Crystal structure determination

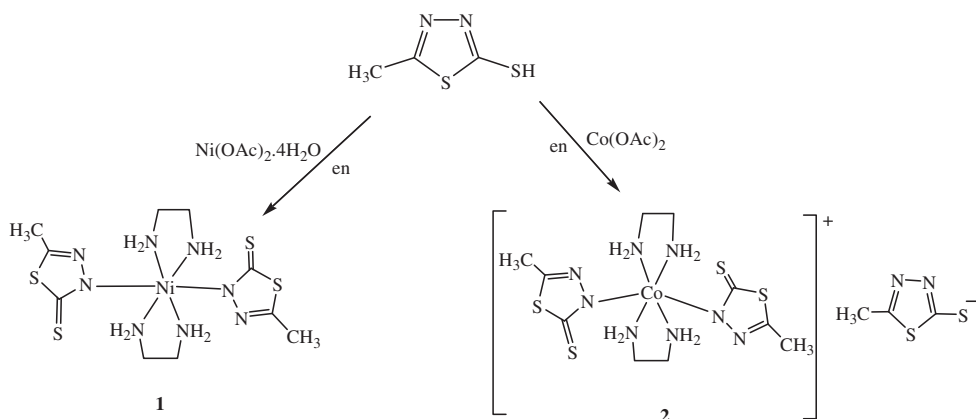
Data collection for complexes was performed on an Oxford Diffraction Gemini diffractometer equipped with CrysAlis Pro. using graphite monochromated MoK $\alpha$  ( $\lambda = 0.71073 \text{ \AA}$ ) radiation. The structures were solved by direct methods (SHELXL-2008) and refined against all data by full matrix least-squares on  $F^2$  using anisotropic displacement parameters for all non-hydrogen atoms. All hydrogens were included in the refinement at geometrically ideal positions and refined with a riding model [17]. The MERCURY package and ORTEP-3 for Windows were used for analysis of the structures and drawing of the figures [18, 19].

## 2.6. Quantum chemical calculation

All calculations were performed using the Gaussian 03 and Gauss View 4.1 [20] program. Structure optimization has been done by the DFT method for isolated molecules in the gaseous phase with Becke's three parameter hybrid exchange functional and the Lee-Yang-Parr correlation functional (B3LYP) and basis sets 6-311 G(d,p){C,H,N,O,S}/Lanl2DZ{M=Ni and Co}. This method was chosen because it combines a relatively low computational cost with a relatively high accuracy and the basis set Lanl2DZ serves the purpose of including the pseudo-potential of the core electrons of the metal [21]. Input geometry for the ligand, **1** and **2** for the DFT calculations were generated from single-crystal X-ray data. Optimized geometrical parameters have been compared with single-crystal X-ray diffraction data. Molecular electrostatic potential mapped surface of the molecules are calculated by DFT/B3LYP/6-311 G(d,p){C,H,N,O,S}/Lanl2DZ{M=Ni and Co} at 0.02 isovalues and 0.004 density values. The red- and blue-colored schemes of MEP are negative and positive electrostatic potentials, respectively. The red region shows atoms with lone pairs; the intensity of the color is proportional to the absolute value of the potential energy. Frontier molecular orbital is also calculated at the same theory level. The positive phase is red and the negative one is green [22].

## 3. Results and discussion

Metal acetates (M=Ni and Co) react with Hmtt and then with en to yield **1** and **2**, respectively. Scheme 1 depicts the formation of complexes which contain 5-methyl-1,3,4-thiadiazole-2-thione and en. Single-crystal X-ray diffraction data indicate that Hmtt is uninegative monodentate, bonding through the thiadiazole ring nitrogen forming octahedral complexes. Both complexes are air stable, non-hygroscopic crystalline solids, which are partially soluble in common organic solvents but soluble in DMF and DMSO, and can be kept in



Scheme 1. Preparation of Ni(II) and Co(III) complexes.

desiccators over a prolonged period without any sign of decomposition. Complexes **1** and **2** melt at 196 and 236 °C, respectively.

### 3.1. IR spectra

The ligand 5-methyl-1,3,4-thiadiazole-2-thiol shows absorption bands at 2868 and 1590  $\text{cm}^{-1}$  due to  $\nu(\text{SH})$  and  $\nu(\text{C}=\text{N})$ , respectively. The disappearance of  $\nu(\text{SH})$  in the spectrum of **1** and the presence of bands at 1598 and 932  $\text{cm}^{-1}$  due to  $\nu(\text{C}=\text{N})$  of the thiadiazole ring and  $\nu(\text{C}=\text{S})$ , respectively, indicate that the nickel ion is bound to the thiadiazole ring nitrogen after loss of a proton on thiol–thione tautomerization. A new band at 3214  $\text{cm}^{-1}$  is due to the N–H stretch of en while being devoid of any peak due to  $\nu(\text{NH})$  of the ligand. A new band at 534  $\text{cm}^{-1}$  due to  $\nu(\text{Ni}-\text{N}_{\text{en}})$  indicates formation of a chelate ring and bonding of en to nickel(II). The IR spectrum of **2** shows a band at 3206  $\text{cm}^{-1}$  due to the N–H stretch of en. The disappearance of  $\nu(\text{SH})$  shows removal of the proton from  $-\text{SH}$ , and appearance of a new band at 548  $\text{cm}^{-1}$  due to  $\nu(\text{Co}-\text{N}_{\text{en}})$  suggests formation of a chelate with ethylenediamine [23].

### 3.2. Electronic spectra and magnetic moments

A magnetic moment of 2.85 BM for  $[\text{Ni}(\text{mtt})_2(\text{en})_2]$  (**1**) and the presence of two bands at 20,162 and 22,988  $\text{cm}^{-1}$  assigned to the  ${}^3A_{2g} \rightarrow {}^3T_{1g}(\text{F})$  ( $\nu_2$ ) and  ${}^3T_{1g}(\text{P})$  ( $\nu_3$ ) transitions, respectively, suggest a distorted octahedral geometry for the complex.  $[\text{Co}(\text{mtt})_2(\text{en})_2](\text{mtt})$  is diamagnetic indicating the presence of Co(III) in low-spin octahedral geometry. It shows bands at 21,740 and 23,040  $\text{cm}^{-1}$  in the visible region which may be attributed to the  ${}^1A_{1g} \rightarrow {}^1E_g$  and  ${}^1A_{1g} \rightarrow {}^1A_{2g}$  transitions, respectively, for low-spin six-coordinate octahedral Co(III). Other high energy bands at 27,462 and 30,123  $\text{cm}^{-1}$  may be assigned to charge transfer/intraligand transitions [24].

### 3.3. Thermal analyses

Thermogram and DTA curves of Hmtt reveal that it is stable to 190 °C and indicates the absence of water in the crystalline phase [25]. Hmtt starts decomposing after its melting

point (188 °C) from 190 to 500 °C (figure S1, see online supplemental material at <http://dx.doi.org/10.1080/00958972.2015.1057131>) and the weight loss could be due to loss of organic moieties in the form of gaseous products through breakage of bonds. The later stage is slower and corresponds to oxidation or vaporization of intermediate products at 390–490 °C, indicating that thermolysis is exothermic. Heating of sample to 700 °C leaves no residue. Thermograms of **1** and **2** show that they are stable to 200 °C (figure S2), indicating the absence of lattice as well as coordinated solvent [16, 26]. The TGA curve of the Ni(II) complex consists of two stages of mass losses, the first weight loss (Calcd; 59.73%, Obs; 60.16%) at 200–400 °C and the second (Calcd; 27.15%, Obs; 27.86%) from 400 to 800 °C could be due to loss of two mtt<sup>−</sup> ligands followed by loss of both en molecules. The intermediate is unstable since the temperature holds on rising; the products lose slight weight at 800–950 °C and finally NiO (Calcd; 12.45%, Obs; 13.16%) is obtained as a residue. A thermogravimetric curve of the Co(III) complex consists of three decomposition stages of mass losses 200–225 °C, 250–320 °C, and 400–700 °C. Upon increase of temperature at 200–250 °C, **2** lost uncoordinated mtt<sup>−</sup> initially; the loss of one en and two mtt<sup>−</sup> (Calcd; 65.58%, Obs; 66.26%) occur in the second step at 250–320 °C and the remaining en moiety is lost from 400 to 700 °C. The latter step is slower and corresponds to oxidation of the intermediate in the form of gaseous products, indicating that thermolysis is exothermic and finally up to 900 °C cobalt oxide (Co<sub>2</sub>O<sub>3</sub>) (Calcd; 9.58%, Obs; 10.26%) is left as a residue.

### 3.4. Antibacterial activity

The antibacterial activities of Hmtt, complexes and commercial antibacterial drugs streptomycin sulfate and neomycin sulfate were tested against five human bacterial pathogens, *Salmonella typhi* (MTCC 3216), *S. flexneri* (ATCC 12022), *S. aureus* (ATCC 25323), *Aeromonas hydrophila* (ATCC 7966), and *E. faecalis* (ATCC 25923), and the results (inhibition zones) are given in table S1. The ligand and the complexes were active against all pathogens at higher concentrations. The highest zone of inhibition (2.5 cm) was recorded for **2** against *S. typhi* and *A. hydrophila* at 50 µg/disc. Co(III) complex is more effective than that of free ligand and the Ni(II) complex. Activities of the ligand and the complexes are lower than streptomycin sulfate and neomycin sulfate. The zone of inhibition area is somewhat larger for the complexes than for free ligand. The activity increases with concentration of the metal complexes, since the concentration plays a vital role in increasing the degree of inhibition [27, 28]. The minimum inhibitory concentrations (MIC) are given in table 1. Complex **2** was most effective against all pathogens with low MIC values in comparison to Hmtt and **1**. The results of antibacterial activity studies clearly indicate that the ligand and complexes are biologically active against all tested bacterial pathogens.

Table 1. MIC of Hmtt, **1**, and **2** against different human bacterial pathogens.

Test bacterium	MIC (µg/mL)		
	Hmtt	<b>1</b>	<b>2</b>
<i>Salmonella typhi</i> (MTCC 3216)	69.96	47.68	21.25
<i>Shigella flexneri</i> (ATCC 12022)	62.85	50.18	28.32
<i>Staphylococcus aureus</i> (ATCC 25323)	84.97	43.20	27.90
<i>Aeromonas hydrophila</i> (ATCC 7966)	114.68	87.33	61.12
<i>Enterococcus faecalis</i> (ATCC 25923)	74.57	53.85	33.62

Table 2. Crystal data collection and structure refinement parameters for **1** and **2**.

Parameters	<b>1</b>	<b>2</b>
Formula	C <sub>10</sub> H <sub>22</sub> N <sub>8</sub> NiS <sub>4</sub>	C <sub>13</sub> H <sub>25</sub> CoN <sub>10</sub> S <sub>6</sub>
Formula weight	441.33	572.78
Crystal system	Monoclinic	Orthorhombic
Space group	<i>P</i> 21/ <i>n</i>	<i>P</i> 21 21 21
<i>T</i> (K)	293(2)	293(2)
$\lambda$ , Mo K $\alpha$ (Å)	0.71073	0.71073
<i>a</i> (Å)	8.6615(3)	9.9649(6)
<i>b</i> (Å)	19.0255(6)	11.5311(5)
<i>c</i> (Å)	11.3820(6)	21.6494(11)
$\alpha$ (°)	90.00	90.00
$\beta$ (°)	103.951(4)	90.00
$\gamma$ (°)	90.00	90.00
<i>V</i> (Å <sup>3</sup> )	1820.31(13)	2487.7(2)
<i>Z</i>	4	4
$\rho$ calcd (g/cm <sup>3</sup> )	1.610	1.529
$\mu$ (mm <sup>-1</sup> )	1.535	1.216
<i>F</i> (0 0 0)	920	1184
Crystal size (mm <sup>3</sup> )	0.28 × 0.25 × 0.22	0.26 × 0.23 × 0.21
$\theta$ range for data collections (°)	3.23–29.12	3.29–29.12
Index ranges	–11 ≤ <i>h</i> ≤ 11 –25 ≤ <i>k</i> ≤ 26 –9 ≤ <i>l</i> ≤ 15	–10 ≤ <i>h</i> ≤ 13 –14 ≤ <i>k</i> ≤ 15 –28 ≤ <i>l</i> ≤ 29
No. of reflections collected	8901	9555
No. of independent reflections ( <i>R</i> <sub>int</sub> )	4886	6702
No. of data/restraints/parameters	4164/0/208	5391/0/271
Goodness-of-fit on <i>F</i> <sup>2</sup>	1.106	0.925
<i>R</i> <sub>1</sub> <sup>a</sup> , <i>wR</i> <sub>2</sub> <sup>b</sup> [ <i>I</i> > 2 $\sigma$ ( <i>I</i> )]	0.0409, 0.1031	0.0641, 0.1805
<i>R</i> <sub>1</sub> <sup>a</sup> , <i>wR</i> <sub>2</sub> <sup>b</sup> (all data)	0.0614, 0.1343	0.0995, 0.2312
Largest difference peak/hole (e Å <sup>-3</sup> )	0.532, –0.457	0.653, –0.429

$$^a R_1 = \sum ||F_o| - |F_c|| / \sum |F_o|; ^b R_2 = \left[ \frac{\sum w(|F_o|^2 - |F_c|^2)^2}{\sum w|F_o|^2} \right]^{1/2}$$

### 3.5. Crystal structure description

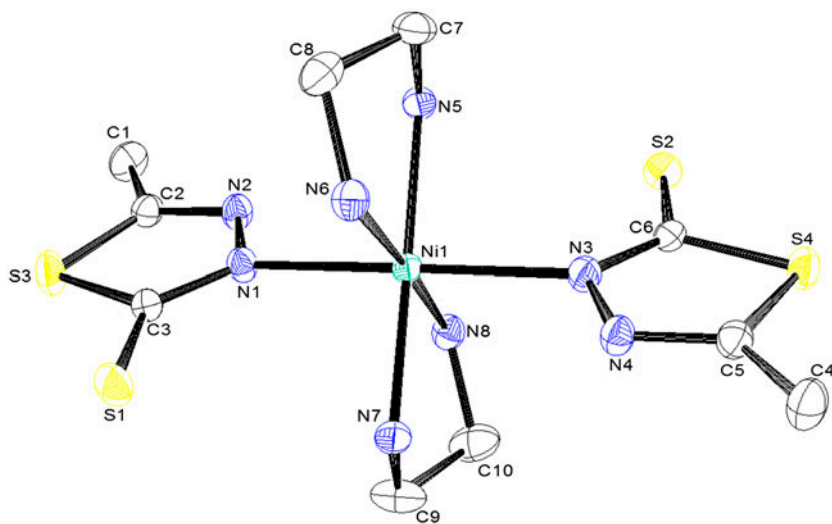
The crystallographic data and structural refinement details for **1** and **2** are given in table 2 and selected bond lengths and angles in table 3. Hydrogen bonding parameters are given in table S2. Figures 1 and 2 show the ORTEP diagram of **1** and **2**, respectively, with the atom numbering scheme.

**3.5.1. Crystal structure description of [Ni(mtt)<sub>2</sub>(en)<sub>2</sub>] (1) and [Co(mtt)<sub>2</sub>(en)<sub>2</sub>](mtt) (2).** The molecular structure of **1** shows that the six-coordinate Ni(II) is bound to four nitrogens of two en at equatorial positions and two thiadiazole nitrogens of 5-methyl-1,3,4-thiadiazole-2-thione at axial positions (figure 1). The crystal structure of **2** consists of [Co(mtt)<sub>2</sub>(en)<sub>2</sub>]<sup>+</sup> and a mtt<sup>–</sup> anion. In the complex unit, Co(III) is bound to two ethylenediamine molecules and two 5-methyl-1,3,4-thiadiazole-2-thione anions via thiadiazole ring nitrogen at the axial positions (figure 2). The axial and equatorial M–N (M=Ni and Co) distances (table 3) suggest an axially distorted octahedral geometry for both complexes and the distances in **2** are longer than **1**. The bite angles for the MC<sub>2</sub>N<sub>4</sub> five-membered rings for **1** are 82.76(13)° and 82.68(13)° and for **2** are 85.4(3)° and 85.1(3)°, indicating substantial distortion in both molecules. The elements of the structure are joined to each other in the crystal packing by an extended system of H-bonds, where hydrogens of ethylenediamine



Table 3. Bond lengths (Å) and angles (°) for **1** and **2**.

Bond lengths (Å)			Bond angles (°)		
	(Exp.)	(Cal.)		(Exp.)	(Cal.)
<b>Complex 1</b>					
Ni–N(1)	2.165(3)	2.167	N7–Ni–N5	177.84(12)	177.87
Ni–N(3)	2.181(3)	2.184	N6–Ni–N8	176.80(13)	176.83
Ni–N(7)	2.080(3)	2.083	N1–Ni–N3	177.09(12)	176.99
Ni–N(5)	2.094(3)	2.096	N7–Ni–N8	82.76(13)	82.78
Ni–N(6)	2.103(3)	2.110	N5–Ni–N6	82.68(13)	82.69
Ni–N(8)	2.114(3)	2.115	N6–Ni–N1	89.82(12)	90.07
S(1)–C(3)	1.690(4)	1.692	N5–Ni–N3	91.38(12)	91.45
S(2)–C(6)	1.699(4)	1.702	N8–Ni–N3	89.32(12)	89.27
N(1)–N(2)	1.388(4)	1.392	N7–Ni–N1	91.67(12)	91.59
<b>Complex 2</b>					
Co–N(1)	1.952(6)	1.953	N2–Co–N3	178.8(3)	178.90
Co–N(2)	1.951(6)	1.948	N8–Co–N5	179.6(3)	179.61
Co–N(3)	1.963(6)	1.966	N4–Co–N1	179.5(3)	179.62
Co–N(4)	1.960(6)	1.964	N4–Co–N3	85.4(3)	85.44
Co–N(5)	1.952(6)	1.948	N2–Co–N1	85.1(3)	85.15
Co–N(8)	1.954(6)	1.950	N2–Co–N8	90.0(3)	90.17
S(2)–C(7)	1.708(8)	1.712	N5–Co–N1	91.0(3)	91.11
S(6)–C(12)	1.723(8)	1.719	N3–Co–N8	91.1(3)	90.98
N(6)–N(5)	1.393(9)	1.395	N3 Co1 N5	89.3(3)	89.6
N(7)–N(8)	1.395(8)	1.402	N4–Co–N8	90.5(3)	90.46

Figure 1. ORTEP diagram of  $[\text{Ni}(\text{mtt})_2(\text{en})_2]$ .

participate in the structure. In the solid state, **1** is stabilized *via* intermolecular N–H $\cdots$ S interaction between the thione sulfur and NH $_2$  hydrogens of ethylenediamine and C–H $\cdots$ S interaction between the thiadiazole ring sulfur and CH hydrogen of a nearby ethylenediamine leading to formation of a linear structure (figure S3). The monomeric units of  $[\text{Co}(\text{mtt})_2(\text{en})_2](\text{mtt})$  are held together through C–H $\cdots$ S, N–H $\cdots$ S, C–H $\cdots$ N, and N–H $\cdots$ N

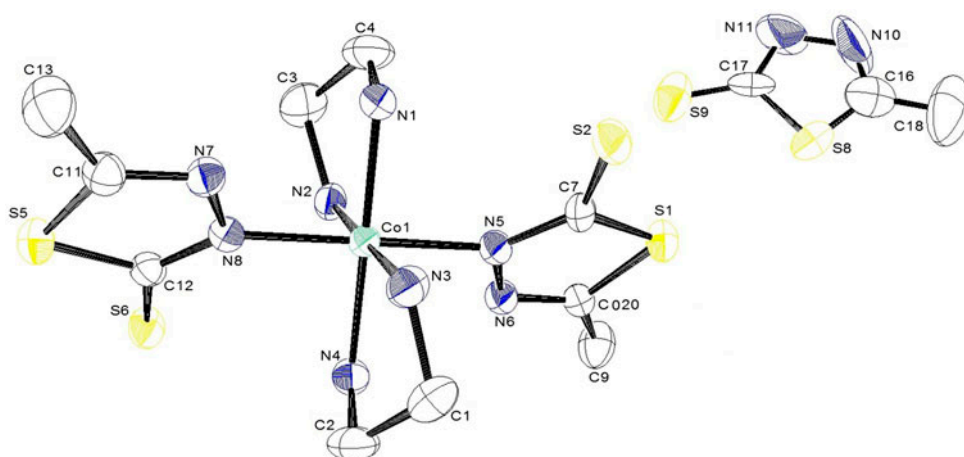


Figure 2. ORTEP diagram of  $[\text{Co}(\text{mtt})_2(\text{en})_2](\text{mtt})$ .

intermolecular hydrogen bonds (figure S4), leading to parallel arrangement of metal-organic framework along the  $a$  axis (figure S5). Uncoordinated mtt anions point toward the space between the adjacent sublayers and occupy interchain positions providing appropriate charge balance which helps to connect three  $[\text{Co}(\text{mtt})_2(\text{en})_2]^+$  cations via  $\text{C}-\text{H}\cdots\text{S}$  and  $\text{C}-\text{H}\cdots\text{N}$  hydrogen bonds between thione sulfur, thiadiazole ring nitrogens with CH hydrogen of methyl, and CH hydrogen of an adjacent en. These interactions with adjacent molecules grow an infinite 3-D framework structure. Complex **2** is stabilized by weak  $\pi\cdots\pi$  interactions occurring between the thiadiazole ring of a complex molecule and thiadiazole ring of a nearby free ligand (figure S6). The above-observed intermolecular hydrogen bonding stabilized the crystal packing giving a supramolecular network. The geometry and bonding parameters agree with those of other Ni/Co complexes containing ethylenediamine [29, 30]. The soft donor site of the  $\text{mtt}^-$  ligand shows no tendency for coordination with Ni(II) and Co(III), as they are hard metal ions and prefer to bind with comparatively hard nitrogen of the ligand.

### 3.6. DFT calculations of ligand, 1 and 2

**3.6.1. Geometry optimization.** Geometry optimizations for the ligand, **1** and **2** have been performed to understand chemical reactivity and to predict the outcome of molecular interactions. The optimized energies (negative values) of the ligand and complexes have been calculated and are shown in table 3, which indicates their stability. There is good agreement between the geometrical parameters obtained by X-ray crystallography and those generated by DFT method (table 3). The calculated carbon–sulfur bond length of the ligand (1.766 Å) decreases in the complexes since sulfur is present in complexes in thione form. The carbon–sulfur bond distances present in both units of the ligand in **1** and **2** are 1.692 Å and 1.712 Å, respectively, suggesting that the carbon sulfur bonds are intermediate between single and double bonds. This trend is also observed in X-ray crystallography. The structure obtained from geometry optimization confirms the distorted geometry around Ni and Co as determined by X-ray diffraction analyses. A comparison of the X-ray structures of the

compounds with their optimized counterparts shows slight conformational discrepancies between them. The Ni–N<sub>(thiadiazole)</sub> and Ni–N<sub>(en)</sub> bond lengths in the coordination sphere are 2.165(3) and 2.094(3) Å in the X-ray structure, whereas the corresponding values in optimized geometries are 2.167 and 2.110 Å. The calculated bond lengths around Co show that Co–N<sub>(thiadiazole)</sub> and Co–N<sub>(en)</sub> bond lengths are 1.952(6) and 1.960(6) Å in X-ray structure, whereas the corresponding values in optimized geometries are 1.950 and 1.964 Å, respectively. Within the chelate rings, the M–N<sub>en</sub> bond distances are shorter than those of M–N<sub>mtt</sub> (table 3), which indicate that the thiadiazole ring nitrogens bond weaker than the en nitrogens. Both complexes involve two five-membered chelate rings, C<sub>2</sub>N<sub>2</sub>M, with calculated bite angles of 82.78° and 85.44° for **1** and **2**, respectively, which represent a deviation from the octahedral geometry. The discrepancies in bond lengths and angles are attributable to H-bonding and packing interactions within the lattice, which are not modeled during computational studies [2, 16]. The deviations in geometrical parameters are due to the fact that the DFT calculations are done for an isolated molecule in gaseous phase, while the X-ray crystallographic data were obtained from crystal lattice of complex molecules [31]. Optimized geometry of the ligand, **1** and **2** are shown in figures S7, S8, and S9. From Mullikan charge distribution on atoms of Hmtt and its complexes, we observed that the charges on the ligand redistributed, as a result of complex formation. The charge on the thiadiazole ring nitrogen which is bonded to metal shifts to higher values {–0.247 [ligand], –0.079 [Ni(II)], and –0.122 [Co(III)]} whereas charge on the thiol sulfur (0.068) shifts to negative value in thione form of complexes {–0.178 [Ni(II)] and –0.124 [Co(III)]}. The carbon atomic charges were either positive or negative. The Mullikan charge distribution on atoms of **1** and **2** are shown in figures 3a and 3b and that of the ligand in figure S10.

**3.6.2. Molecular electrostatic potential (MEP).** To predict reactive sites for electrophilic and nucleophilic processes, electrostatic surface potentials were obtained at the B3LYP/6–311G(d,p)/LanL2DZ optimized geometry. The different values of the electrostatic potential

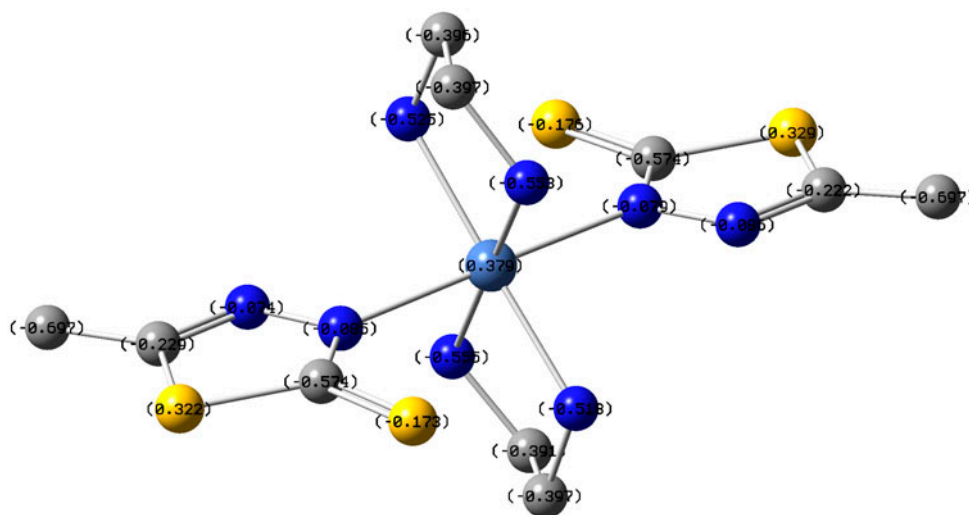


Figure 3a. Charge distribution on atoms of [Ni(mtt)<sub>2</sub>(en)<sub>2</sub>] (hydrogens are omitted for clarity).

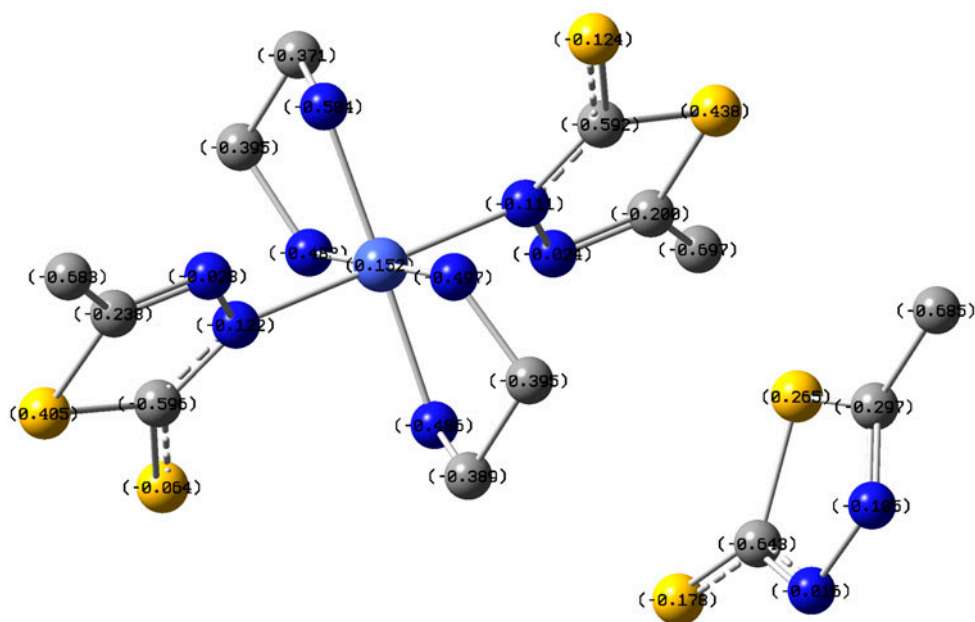


Figure 3b. Charge distribution on atoms of  $[\text{Co}(\text{mtt})_2(\text{en})_2](\text{mtt})$  (hydrogens are omitted for clarity).

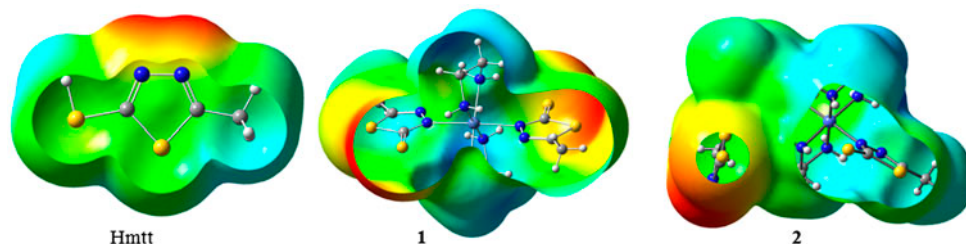


Figure 3c. MEP plots of Hmtt, **1**, and **2**.

at the surface are represented by different colors and the potential increases in the order: red < orange < yellow < green < blue. The negative red regions of MEP were related to electrophilic reactivity and the positive (blue) ones to nucleophilic reactivity. Negative (red) regions in Hmtt are found over the thiadiazole ring nitrogens and positive regions (blue) around hydrogens. Thus, it would be predicted that an electrophile would preferentially attack the ligand at the nitrogen positions. According to the calculated results (figure 3c), the MEP map of **1** shows that the negative potential sites are around thione sulfur and the positive potential sites are around the hydrogens (more on en). The red regions are over  $\text{mtt}^-$  in **2**, but not on thione sulfur in the coordination sphere. The red regions decrease in complexes, indicating that the thiol form is converted to thione form. The green areas cover parts of the molecule where electrostatic potentials are close to zero (C–C, C–N, and C–S bonds). These sites give information about the region where the compound can have noncovalent interactions [32].

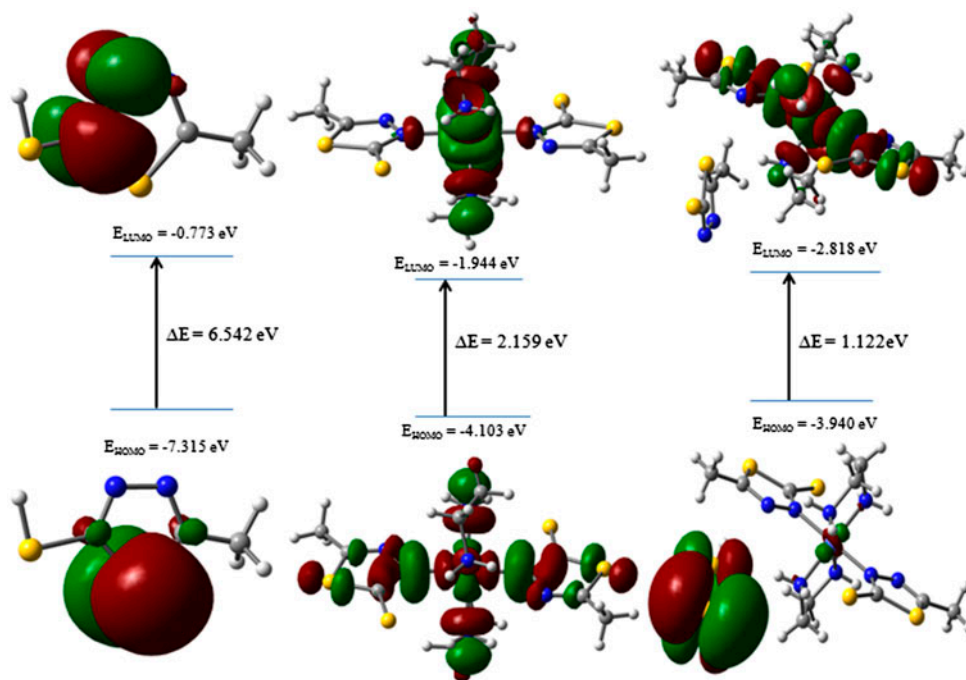


Figure 3d. FMO diagrams of Hmtt and its Ni(II) and Co(III) complexes.

**3.6.3. Frontier molecular orbital (FMO) analysis.** The HOMO energy characterizes the ability for electron donation, the LUMO characterizes the ability of electron acceptance, and the gap between HOMO and LUMO characterizes the molecular chemical stability. The HOMO-LUMO energy and the energy gap ( $\Delta E$ ) for Hmtt and complexes have been calculated at DFT/B3LYP/6-311G(d,p)/Lan12DZ level [33] and the results are given in table 4. 3-D plots of the HOMO and LUMO for Hmtt, **1** and **2** are shown in figure 3d. The HOMO is mainly located at the thiadiazole ring sulfur and the LUMO electron density is located on thiadiazole ring nitrogen. This means that the electron acceptor is the thiadiazole ring nitrogen. The positive phase is red and the negative one is green. It is clear from the figure that the HOMOs are localized mainly on the thiadiazole ring with a little contribution from *en*. On the other hand, the LUMOs are localized mainly on *en* but not on thiadiazole ring in **1**. In **2**, the  $\text{mtt}^-$  makes more contribution of electron density to HOMO, whereas in LUMO the anion part does not make any contribution. The LUMOs are mainly localized

Table 4. Calculated dipole moment, optimized energy, and FMO energies for Hmtt, **1**, and **2**.

Compound	Dipole moment (Debye)	Optimized energy (Hartree)	Energies (eV)			Degree of hardness $\eta$
			HOMO	LUMO	$\Delta E$	
Hmtt	2.102	-1022.583	-7.315	-0.773	6.542	3.271
<b>1</b>	0.753	-1041.587	-4.103	-1.944	2.159	1.080
<b>2</b>	21.837	-1262.988	-3.940	-2.818	1.122	0.561

on thiadiazole ring and *en* which are bonded to cobalt. The value of the energy separation between the HOMO and LUMO is about three and six times lower for **1** and **2**, respectively, than that of free Hmtt. The small HOMO–LUMO energy gap means low excitation energy, good stability, and a low chemical hardness for the complex. The electronic transition from the ground state to the excited state due to transfer of electrons from the HOMO to LUMO is mainly due to  $\pi \cdot \pi$  transition.

The chemical hardness of a molecule is defined by the formula [34]

$$\eta = \{-E_{\text{HOMO}} + E_{\text{LUMO}}\}/2$$

where  $E_{\text{HOMO}}$  and  $E_{\text{LUMO}}$  are the energies of the HOMO and LUMO. The values of  $\eta$  for Hmtt, **1** and **2** are 3.271, 1.080, and 0.561 eV, respectively, which indicate that Hmtt is a hard material, whereas the complexes are soft materials with **2** being softer than **1**. The above result is supported by the presence of UV–vis bands at 446, 415, and 324 nm for **1** and at 460, 434, and 332 nm for **2** which indicates that **2** is softer than **1**. The non-linear optical (NLO) property of materials associated with the delocalized  $\pi$ -electrons of a molecule plays an important role in the design of materials used in communication technology and optical devices [35]. An increase in delocalization of electron on the molecule results in change in the NLO properties which in turn are related to the energy gap between HOMO and LUMO. The addition of mtt in **2** and various intermolecular hydrogen bonds could affect the nonlinear optical properties by changing the energy gap between HOMO and LUMO, where the low HOMO–LUMO gap requires small excitation energy and so the absorption bands of a molecule are shifted toward the visible region [36]. Due to the presence of various types of hydrogen bonding in **2**, electron delocalization becomes easier, which decreases the value of the energy gap, so the absorption bands in the electronic spectrum are shifted toward the visible region and, consequently, increases the NLO properties as compared to **1**. This suggests that the  $\text{mtt}^-$  modifies the charge distribution of the  $\pi$ -electron structure *versus* that of the Ni(II) complex. The uncoordinated  $\text{mtt}^-$  plays the role of structural unit, which enhances the overall intermolecular interactions and affects the electron transfer between donor and acceptor groups. Due to these properties, **2** may be used as an optoelectronic material.

### 3.7. Electrochemical behavior of $[\text{Ni}(\text{mtt})_2(\text{en})_2]$ (**1**) and $[\text{Co}(\text{mtt})_2(\text{en})_2](\text{mtt})$ (**2**)

The electrochemical behavior of **1** and **2** using cyclic voltammetry is depicted in figure 4. The cyclic voltammograms were obtained at a mercury electrode using 0.1 M KCl as supporting electrolyte in the potential range of  $-1.0$ – $1.0$  V with a scan rate of  $100 \text{ mVs}^{-1}$  and show the quasi-reversible and irreversible redox behavior of **1** and **2**, respectively. Complex **1** exhibits cathodic and anodic peak potentials at 0.510 and 0.326 V, respectively, and the separation between the cathodic and anodic peak potentials ( $\Delta E_p = E_{\text{pa}} - E_{\text{pc}}$ ) of 0.184 V indicates a quasi-reversible redox process assignable to the nickel(II)/nickel(III) couple with the formal redox potential  $E = (E_{\text{pa}} + E_{\text{pc}})/2 = 0.418 \text{ V}$  [37]. Complex **2** exhibits cathodic and anodic peak potentials at 0.488 and  $-0.526$  V, respectively, and the separation ( $\Delta E_p = E_{\text{pa}} - E_{\text{pc}}$ ) of 1.014 V indicates an irreversible redox process assignable to the Co(III)/Co(II) couple with the formal redox potential  $E = (E_{\text{pa}} + E_{\text{pc}})/2 = 0.019 \text{ V}$ . However, it is to be noted that the peak separation ( $\Delta E_p = E_{\text{pa}} - E_{\text{pc}}$ ) is somewhat high as compared to that expected for one-electron process and hence it can be concluded that the redox process is coupled with some chemical reaction.

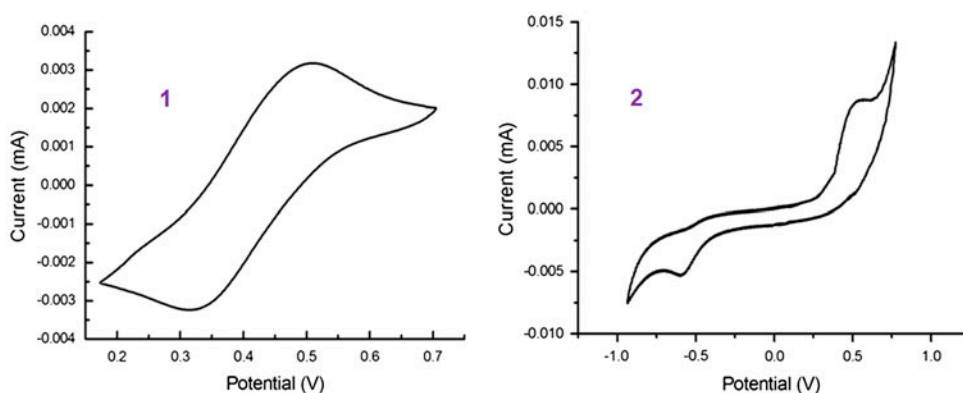


Figure 4. Cyclic voltammograms of **1** and **2**.

#### 4. Conclusion

[Ni(mtt)<sub>2</sub>(en)<sub>2</sub>] (**1**) and [Co(mtt)<sub>2</sub>(en)<sub>2</sub>](mtt) (**2**) have been synthesized and characterized by various physicochemical methods. The crystal structure of **1** is stabilized *via* C–H···S and N–H···S intermolecular interactions, whereas **2** is stabilized by C–H···S, N–H···S and C–H···N and N–H···N interactions. TGA shows that the complexes are stable to 200 °C indicating the absence of lattice as well as coordinated solvent molecules and NiO and Co<sub>2</sub>O<sub>3</sub> are left as a final residue in **1** and **2**, respectively. Structural parameters from crystallographic and DFT studies are consistent with each other. FMOs and NLO analyses reveal that **2** is softer than **1**, as supported by the occurrence of low excitation energy bands for  $\pi \rightarrow \pi^*$  and  $n \rightarrow \pi^*$  transitions, and **2** may be used as an optoelectronic material. The biological results suggest that **2** is more active than free Hmtt and **1**. The complexes show enhanced antibacterial activities against microbial strains in comparison to the free ligand. The results of antibacterial studies suggest that the present complexes have comparable activity to other reported nickel and cobalt complexes. Complex **1** shows quasi-reversible redox process assignable to the Ni(II)/Ni(III), while **2** exhibits irreversible redox behavior for Co(III)/Co(II) couple with the formal redox potentials of 0.418 and 0.019 V, respectively.

#### Supplementary material

CCDC 963587 and 963589 contain the supplementary crystallographic data for [Co(mtt)<sub>2</sub>(en)<sub>2</sub>](mtt) (**2**) and [Ni(mtt)<sub>2</sub>(en)<sub>2</sub>] (**1**), respectively. These data can be obtained free of charge *via* <http://www.ccdc.cam.ac.uk/conts/retrieving.html>, or from the Cambridge Crystallographic Data Center, 12 Union Road, Cambridge CB2 IEZ, UK; Fax: (+44)1223-336-033; or Email: [deposit@ccdc.cam.ac.uk](mailto:deposit@ccdc.cam.ac.uk).

#### Acknowledgements

Dr M.K. Bharty is thankful to the Department of Science and Technology, New Delhi, India for the award of a Young Scientist Project (No. SR/FT/CS-63/2011). Authors are thankful

to Prof. R.N. Kharwar, Department of Botany, Faculty of Science, BHU, for antibacterial activity study.

## Disclosure statement

No potential conflict of interest was reported by the authors.

## References

- [1] B.L. Sharma, S.K. Tandon. *Pharmazie*, **39**, 858 (1984).
- [2] R.K. Dani, M.K. Bharty, S.K. Kushawaha, O. Prakash, R.K. Singh, N.K. Singh. *Polyhedron*, **65**, 31 (2013).
- [3] M. Du, X.-J. Zhao. *J. Mol. Struct.*, **694**, 235 (2004).
- [4] C. Karthick, P. Gurumoorthy, M.A.I. Musthafa, R. Lakra, P.S. Korrapati, A.K. Rahiman. *J. Coord. Chem.*, **67**, 1794 (2014).
- [5] A.M. Rayan, M.M. Ahmed, M.H. Barakat, A.T. Abdelkarim, A.A. El-Sherif. *J. Coord. Chem.*, **68**, 678 (2015).
- [6] S.Y. Ebrahimipour, M. Mohamadi, J. Castro, N. Mollania, H.A. Rudbari, A. Saccá. *J. Coord. Chem.*, **68**, 632 (2015).
- [7] M. Amirnasr, R.S. Sadeghi Erami, K. Mereiter, K.S. Joß, S. Meghdadi, S. Abbasi. *J. Coord. Chem.*, **68**, 616 (2015).
- [8] P. Subbaraj, A. Ramu, N. Raman, J. Dharmaraja. *J. Coord. Chem.*, **67**, 2747 (2014).
- [9] A. Mishra, N.K. Kaushik, A.K. Verma, R. Gupta. *Eur. J. Med. Chem.*, **43**, 2189 (2008).
- [10] D.M. Livermore. *Clin. Infect. Dis.*, **36**, S11 (2003).
- [11] S.T. Zheng, J. Zhang, J.M. Clemente-Juan, D.-Q. Yuan, G.-Y. Yang. *Angew. Chem. Int. Ed.*, **48**, 7176 (2009).
- [12] E.M. Villa, C.A. Ohlin, E. Balogh, T.M. Anderson, M.D. Nyman, W.H. Casey. *Angew. Chem. Int. Ed.*, **47**, 4844 (2008).
- [13] F. Hipler, R.A. Fischer, J. Müller. *J. Chem. Soc., Perkin Trans.*, **2**, 1620 (2002).
- [14] P. Bharati, A. Bharti, M.K. Bharty, S. Kashyap, U.P. Singh, N.K. Singh. *Polyhedron*, **63**, 222 (2013).
- [15] A.W. Bauer, W.M. Kirby, J.C. Sherris, M. Turck. *Am. J. Clin. Pathol.*, **45**, 493 (1966).
- [16] S.K. Kushawaha, R.K. Dani, M.K. Bharty, U.K. Chaudhari, V.K. Sharma, R.N. Kharwar, N.K. Singh. *J. Mol. Struct.*, **1063**, 60 (2014).
- [17] G.M. Sheldrick. *Acta Crystallogr., Sect. A: Found. Crystallogr.*, **64**, 112 (2008).
- [18] I.J. Bruno, J.C. Cole, P.R. Edgington, M. Kessler, C.F. Macrae, P. McCabe, J. Pearson, R. Taylor. *Acta Crystallogr., Sect. B: Struct. Sci.*, **58**, 389 (2002).
- [19] L.J.J. Farrugia. *J. Appl. Crystallogr.*, **30**, 565 (1997).
- [20] M.J. Frisch, G.W. Trucks, H.B. Schlegel, G.E. Scuseria, M.A. Robb, J.R. Cheeseman, V.G. Zakrzewski, J.A. Montgomery, R.E. Stratmann, J.C. Burant, S. Dapprich, J.M. Millam, A.D. Daniels, K.N. Kudin, M.C. Strain, O. Farkas, J.B.V. Tomasi, M. Cossi, R. Cammi, B. Mennucci, C. Pomelli, C. Adamo, S. Clifford, J. Ochterski, G.A. Petersson, P.Y. Ayala, Q. Cui, D.K. Morokuma, A.D. Malick, K. Rabuck, J.B. Raghavachari, J. Foresman, J. Cioslowski, J.V. Ortiz, A.G. Baboul, B.B. Stefanov, G.L.A. Liu, P. Piskorz, I. Komaromi, R. Gomperts, R.L. Martin, D.J. Fox, T. Keith, M.A. Al-Laham, C.Y. Peng, A. Nanayakkara, M. Challacombe, P.M.W. Gill, B. Johnson, W. Chen, M.W. Wong, J.L. Andres, C. Gonzalez, M. Head-Gordon, E.S. Replogle, J.A. Pople, Gaussian 03, Revision A.1, Gaussian, Inc., Pittsburgh (2003).
- [21] A.D. Becke. *J. Chem. Phys.*, **98**, 5648 (1993).
- [22] C. Lee, W. Yang, R.G. Parr. *Phys. Rev. B*, **37**, 785 (1988).
- [23] K. Nakamoto. *Infrared and Raman Spectra of Inorganic and Coordination Compounds*, 4th Edn, Wiley Interscience, New York (1986).
- [24] A.B.P. Lever. *Inorganic Electronic Spectroscopy*, 2nd Edn, Elsevier, Amsterdam (1984).
- [25] A.V. Nikolaev, V.A. Logvienko, L.T. Myachina. *Thermal Analysis*, Vol. 2, p. 779, Academic Press, New York (1969).
- [26] A.H. Kianfar, L. Keramat, M. Dostani, M. Shamsipur, M. Roushani, F. Nikpour. *Spectrochim. Acta, Part A*, **77**, 424 (2010).
- [27] R.S. Srivastava. *Inorg. Chim. Acta*, **56**, L65 (1981).
- [28] W.E. Levinson, E. Jawetz. *Medical Microbiology and Immunology*, 4th Edn, Appleton & Lange, Stamford (1996).
- [29] N.K. Singh, M.K. Bharty, R. Dulare, R.J. Butcher. *Polyhedron*, **28**, 2443 (2009).
- [30] P.J. Squattrito, T. Iwamoto, S.-I. Nishikiori. *Chem. Commun.*, 2665 (1996).



- [31] J.B. Foresman, A. Frisch. *Exploring Chemistry with Electronic Structure methods*, 2nd Edn, Gaussian Inc., Pittsburgh, PA (1996).
- [32] J.S. Murray, K. Sen. *Molecular Electrostatic Potentials Concepts and Applications*, Elsevier, Amsterdam (1996).
- [33] D. Zhenming, S. Heping, L. Yufang, L. Diansheng, L. Bo. *Spectrochim. Acta, Part A*, **78**, 1143 (2011).
- [34] K. Fukui. *Science*, **218**, 747 (1982).
- [35] D. Sajan, H. Joe, V.S. Jayakumar, J. Zaleski. *J. Mol. Struct.*, **785**, 43 (2006).
- [36] R.G. Pearson. *Proc. Nat. Acad. Sci.*, **83**, 8440 (1986).
- [37] J. Taraszewska, K. Zięba, J. Kowalski, B. Korybut-Daszkiewicz. *Electrochim. Acta*, **53**, 3531 (2008).